# Assessment of a Recent Thin-Layer Method for Measuring the Rates of Electron Transfer across Liquid/Liquid Interfaces

**Anna L. Barker and Patrick R. Unwin***

*Department of Chemistry, University of Warwick, Coventry CV4 7AL, U.K.*

*Received: September 21, 1999*

A quantitative model has been developed for a recently introduced thin-layer method (Shi, C.; Anson, F. C. *J. Phys. Chem. B* **1998**, *102*, 9850; **1999**, *103*, 6283) for measuring the rate constants of electron transfer (ET) at the interface between two immiscible electrolyte solutions (ITIES). In this method a macroscopic graphite electrode is coated with a thin organic (nitrobenzene) film (phase 1) containing one redox-active species, which is immersed in a second immiscible (aqueous) phase (2) containing a different redox species, which is insoluble in phase 1. The model predicts the voltammetric response for ET processes at the ITIES, irrespective of the concentrations of reactants in the two phases. Results from the model show that an earlier approximate treatment of the method is rarely applicable for typical experimental parameters reported hitherto. The approximate method is only reliable when there is considerable excess of reactant in phase 2. Under these conditions, the current response for a bimolecular ET rate constant of 1 cm $M^{-1}$ $s^{-1}$ can barely be distinguished from a diffusion-controlled process. The conclusions drawn from earlier experimental studies, suggesting that ET is independent of the potential drop across the ITIES, may be a consequence of this diffusional limitation. It is demonstrated that there are advantages to decreasing the concentration of reactant in phase 2, and in using a wide range of potential scan rates, to facilitate the determination of larger ET rate constants by this method.

## Introduction

The importance of understanding electron transfer (ET) reactions at the interface between two immiscible electrolyte solutions (ITIES) is now well-recognized.[1] Considerable interest has been generated in studying these processes as simple models for redox reactions occurring at biological membranes,[2−4] as well as representing a valuable intermediate case between homogeneous ET in solution and heterogeneous ET at the solid electrode/solution interface.[5] Although several theoretical treatments have been proposed for ET across liquid/liquid interfaces,[5−8] relatively few experimental studies have been reported. In part, this is due to the considerable technical difficulties that must be overcome to study this type of process by conventional methods, such as cyclic voltammetry. Problems include distortions associated with *iR* drop and double-layer charging currents, as well as the difficulty of discriminating between ET and ion-transfer processes occurring at the interface.

A key question that is currently attracting much attention is whether the rate of interfacial ET processes depends on the potential drop across the interface. In this respect, the literature appears undecided, with some reports suggesting that the rate of ET is insensitive to the potential applied across the interface,[9,10] and others finding there to be a significant potential dependence.[11,12] Recently, progress has been made to resolve this important issue through the development of several novel experimental approaches.[11−15] In particular, scanning electrochemical microscopy (SECM) is providing considerable new insights.[11] A new model[12] now allows the SECM feedback approach to be used without any restriction on the composition of the two phases that was required in earlier SECM studies.

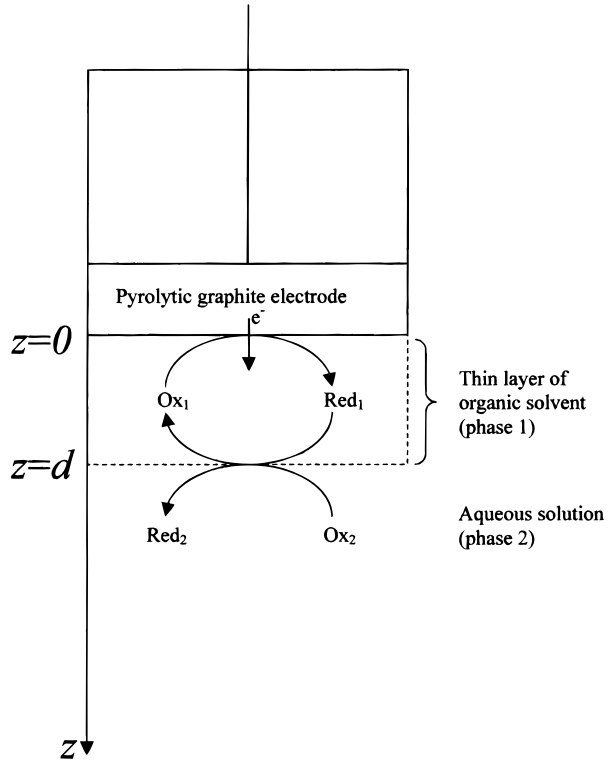


**Figure 1.** Schematic of the working electrode employed in the electrochemical cell of ref 9 to probe electron transfer rates across liquid/liquid interfaces by recording the voltammetric response of reactants dissolved in thin layers of organic solvent adhered to graphite electrodes. This diagram shows the coordinate system for the simulations reported herein.

* Corresponding author. E-mail: p.r.unwin@warwick.ac.uk.

10.1021/jp993373z CCC: $19.00 
Published on Web 02/08/2000

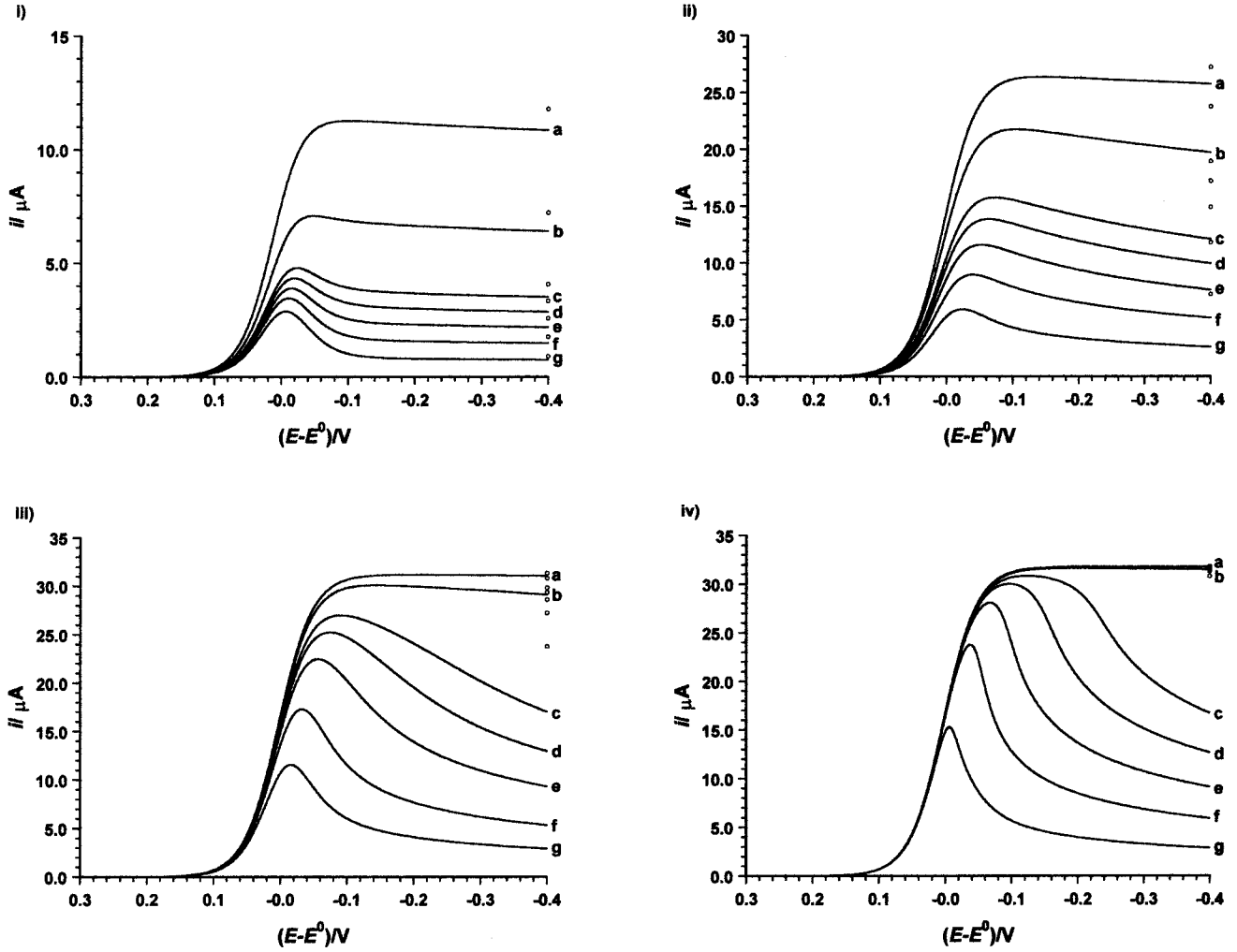


**Figure 2.** Simulated voltammograms for $k_{12}$ = (i) 0.1, (ii) 1.0, (iii) 10.0, and (iv) 100.0 cm $M^{-1}$ $s^{-1}$. In each case, $D_{Ox_1} = D_{Red_1} = 6.0 \times 10^{-6}$ $cm^2$ $s^{-1}$, $D_{Ox_2} = 7.5 \times 10^{-6}$ $cm^2$ $s^{-1}$, $C^*_{Ox_1} = 0.55$ mM, $d = 32$ $\mu$m, $A = 0.32$ $cm^2$, $\upsilon_s = 5$ mV $s^{-1}$, and $K_r$ takes the values (a) 20.0, (b) 10.0, (c) 5.0, (d) 4.0, (e) 3.0, (f) 2.0, and (g) 1.0. The predicted steady-state currents from the constant-composition model, eq 2, for each $K_r$ value are shown as open circles (○). In each of these cases, the highest current data point relates to $K_r = 20$ and decreases with decreasing $K_r$.

This new methodology has advantages over the old method in allowing the characterization of much faster kinetics.

An alternative strategy for investigating the kinetics of ET processes at ITIES has recently been suggested that involves trapping a thin layer of liquid, of nanometer to micrometer dimensions, between an ultramicroelectrode and a second immiscible solvent.[11a] This approach has been developed by Shi and Anson[9] to study ET rates across ITIES by cyclic voltammetry, employing macroscopic graphite electrodes coated with thin (up to 30 $\mu$m) films of an organic solvent such as nitrobenzene (NB). The organic layer contains a redox-active species e.g., $Ox_1$, that can be reduced at the electrode, generating the reduced form, $Red_1$. The electrode, coated with the thin layer, is immersed in an immiscible aqueous solution containing the oxidized form of a second redox couple, $Ox_2$ (Figure 1). The organic film prevents the hydrophilic species, $Ox_2$, in the aqueous phase from being directly reduced at the electrode. If a redox reaction can occur between $Red_1$ and $Ox_2$, a feedback cycle is established in which $Ox_1$ is regenerated in the organic phase, at the ITIES, and can diffuse back to the electrode, enhancing the current signal.

$$\text{ITIES: } \mathrm{Red_1} + \mathrm{Ox_2} \rightarrow \mathrm{Ox_1} + \mathrm{Red_2} \qquad (1)$$

This approach has the advantage of requiring relatively simple instrumentation.[9] Provided that the concentration of $Ox_2$ in the aqueous phase close to the ITIES can be assumed to be constant and equal to its initial bulk value, and that a sufficiently slow scan rate is used, the current is predicted to rise to a plateau indicative of a steady-state concentration profile within the thin layer. Under these conditions the value of the observed plateau current, $i_{obs}$, is governed by the rate of ET across the ITIES and the rate of diffusion of the species in the thin layer.[9b,c,16]

$$\frac{1}{i_{obs}} = \frac{1}{i_D} + \frac{1}{i_{ET}} \qquad (2)$$

in which $i_D$ is the current corresponding to the diffusion-controlled reduction of $Ox_1$ (confined to the thin layer) at the graphite electrode, given by

$$i_D = nFAc^*_{Ox_1}D_{Ox_1}/d \qquad (3)$$

and $i_{ET}$ is a characteristic current corresponding to the ET process across the ITIES.

$$i_{ET} = nFAk_{12}c^*_{Ox_1}c^*_{Ox_2} \qquad (4)$$

In these equations, $n$ is the number of electrons transferred per redox event, $F$ is Faraday's constant, $A$ is the area of the electrode, $c^*_{Ox_1}$ and $c^*_{Ox_2}$ are the initial bulk concentrations of

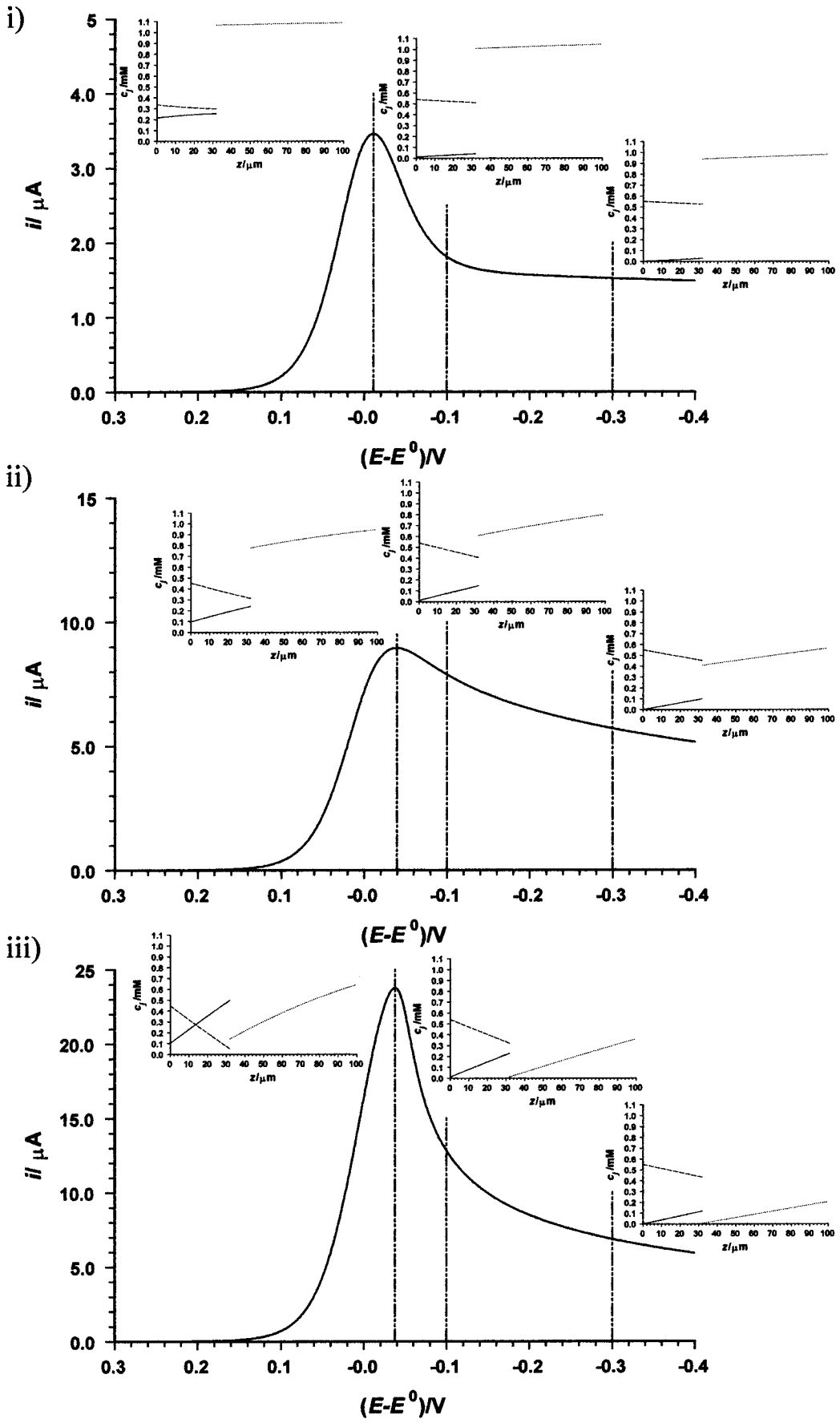


**Figure 3.** Simulated voltammograms for $D_{Ox_1} = D_{Red_1} = 6.0 \times 10^{-6}$ cm$^2$ s$^{-1}$, $D_{Ox_2} = 7.5 \times 10^{-6}$ cm$^2$ s$^{-1}$, $C^*_{Ox_1} = 0.55$ mM, $d = 32$ $\mu$m, $A = 0.32$ cm$^2$, $\upsilon_s = 5$ mV s$^{-1}$, and $K_r = 2$ with $k_{12}$ taking the values (i) 0.1, (ii) 1.0, and (iii) 100.0 cm M$^{-1}$ s$^{-1}$. Insets: concentration profiles of $Ox_1$ (solid line), $Red_1$ (dashed line), and $Ox_2$ (dotted line) as a function of distance from the electrode, $z$, at potentials indicated by the vertical bars and described in the text. ITIES position: $z = 32$ $\mu$m.

$Ox_1$ and $Ox_2$, respectively, $D_{ox_1}$ is the diffusion coefficient of $Ox_1$ in the organic layer, $k_{12}$ is the bimolecular rate constant for the redox reaction at the ITIES, and $d$ is the thickness of the film.

This technique has been used to investigate the rate of ET across the nitrobenzene/aqueous interface between decamethylferrocene or zinc tetraphenylporphyrin radical cation in the organic phase and various aqueous redox species.[9b,c] In these studies, the observed steady-state currents were determined as a function of concentration of the redox mediator in the aqueous phase (keeping the concentration of the species in the organic phase constant) and analyzed in terms of eq 2. The measured rate constants were typically of the order of 1 cm $M^{-1}$ $s^{-1}$ and were apparently insensitive to varying the driving force for the ET process by changing the potential across the ITIES, by altering the concentration of a common supporting electrolyte in the two phases, or by changing the nature of the redox species in the aqueous phase.

In these experiments, the procedure for extracting the rate constant involves measuring the gradient of linear plots of $1/i_{obs}$ vs $1/c_{Ox_2}$ (see eq 2). The accuracy with which $k_{12}$ can be determined is thus highly dependent on the reliability of the data at low concentrations of $Ox_2$ in the aqueous phase. Even when comparable concentrations of $Ox_1$ and $Ox_2$ were employed, it was assumed that there would not be significant depletion of $Ox_2$ at the interface and that the composition of phase 2 could be treated as remaining constant.[9b,c]

The aim of this paper is to develop a full treatment for the planar thin-layer method and identify carefully when eq 2 can be applied. We also assess how the technique could be optimized to facilitate the study of ET kinetics and identify the range of rate constants that should be accessible to study.

**Theory**

The simulation presented below employs standard explicit finite-difference methods to calculate the linear-sweep voltammetric response of a planar working electrode operating in the experimental arrangement illustrated in Figure 1.

Consider a simple reversible electron transfer at the working electrode, for which only reactant $Ox_1$ is initially present in the thin layer at concentration $c^*_{Ox_1}$.

$$Ox_1 + ne^- \rightleftharpoons Red_1 \tag{5}$$

Under conditions where contributions due to convection and migration are negligible, the time-dependent current can be calculated by solving the linear-diffusion equations for each phase

$$0 < z < d \qquad \frac{\partial c_{Ox_1}}{\partial t} = D_{Ox_1}\frac{\partial^2 c_{Ox_1}}{\partial z^2} \tag{6}$$

$$\frac{\partial c_{Red_1}}{\partial t} = D_{Red_1}\frac{\partial^2 c_{Red_1}}{\partial z^2} \tag{7}$$

$$d < z < \infty \qquad \frac{\partial c_{Ox_2}}{\partial t} = D_{Ox_2}\frac{\partial^2 c_{Ox_2}}{\partial z^2} \tag{8}$$

where $c_{Ox_1}$, $c_{Red_1}$, $c_{Ox_2}$ and $D_{Ox_1}$, $D_{Red_1}$, $D_{Ox_2}$ are the concentrations and diffusion coefficients of species $Ox_1$, $Red_1$, and $Ox_2$, respectively, $z$ is the coordinate normal to the electrode surface in the one-dimensional thin-layer geometry, $d$ is the thickness of the thin layer, and $t$ is time.

Since only species $Ox_1$ and $Ox_2$ are present in the thin layer (phase 1) and the bulk solution (phase 2), respectively, prior to the potential scan, the initial condition is

$$t = 0 \qquad c_{Ox_1} = c^*_{Ox_1} \tag{9}$$

$$c_{Red_1} = 0 \tag{10}$$

$$c_{Ox_2} = c^*_{Ox_2} \tag{11}$$

where $c^*_{Ox_2}$ is the initial bulk concentration of $Ox_2$, in phase 2.

The electrode potential is subsequently scanned linearly with time at a rate of $\upsilon_s$ (V $s^{-1}$) from an initial potential, $E_i$. The electrode potential at time $t$ is therefore

$$t > 0 \quad E_t = E_i - \upsilon_s t \tag{12}$$

If the electrode kinetics are sufficiently rapid to ensure species $Ox_1$ and $Red_1$ are always in dynamic equilibrium at the electrode surface, the ratio of the concentrations of oxidized and reduced species at the electrode can be described by the Nernst equation. This assumption is valid for all of the redox couples in the thin layer studied so far.[9] Kinetic effects at the electrode could be considered, but this would complicate the analysis and use of the method in non-steady-state applications. The boundary conditions at the electrode for the problem under consideration can therefore be summarized as follows

$$t > 0, z = 0: \qquad \frac{c_{Ox_1}}{c_{Red_1}} = \exp\left[\left(\frac{nF}{RT}\right)(E_t - E^\circ)\right] \tag{13}$$

$$D_{Ox_1}\frac{\partial c_{Ox_1}}{\partial z} = -D_{Red_1}\frac{\partial c_{Red_1}}{\partial z} \tag{14}$$

in which $E^\circ$ is the standard (strictly, formal) potential of the $Ox_1/Red_1$ couple, $R$ is the gas constant, and $T$ is temperature.

The boundary condition imposed at the ITIES relates the flux of species at that interface to the rate of the second-order redox reaction

$$z = d: \qquad D_{Ox_1}\frac{\partial c_{Ox_1}}{\partial z} = -D_{Red_1}\frac{\partial c_{Red_1}}{\partial z} = D_{Ox_2}\frac{\partial c_{Ox_2}}{\partial z} = k_{12}c_{Red_1}c_{Ox_2} \tag{15}$$

where $k_{12}$ is the interfacial bimolecular rate constant (cm $M^{-1}$ $s^{-1}$) for the reaction at the interface. A further boundary condition specifies that at a semiinfinite distance from the electrode the concentration of species $Ox_2$ remains at its initial bulk concentration, $c^*_{Ox_2}$. The concentration of species $Ox_2$ can be assumed to be unperturbed at a distance of $6\delta$,[17,18] where $\delta$ is the diffusion length given by

$$\delta = \sqrt{D_{Ox_2}t_{total}} \tag{16}$$

in which $t_{total}$ is the total time taken for the scan.

It is straightforward to reformulate the problem to give a general solution through the introduction of the following dimensionless terms.

$$C_j = c_j/c^*_{Ox_1} \qquad \text{where } j \text{ denotes } Ox_1 \text{ or } Red_1 \tag{17}$$

$$C_{Ox_2} = c_{Ox_2}/c^*_{Ox_2} \tag{18}$$

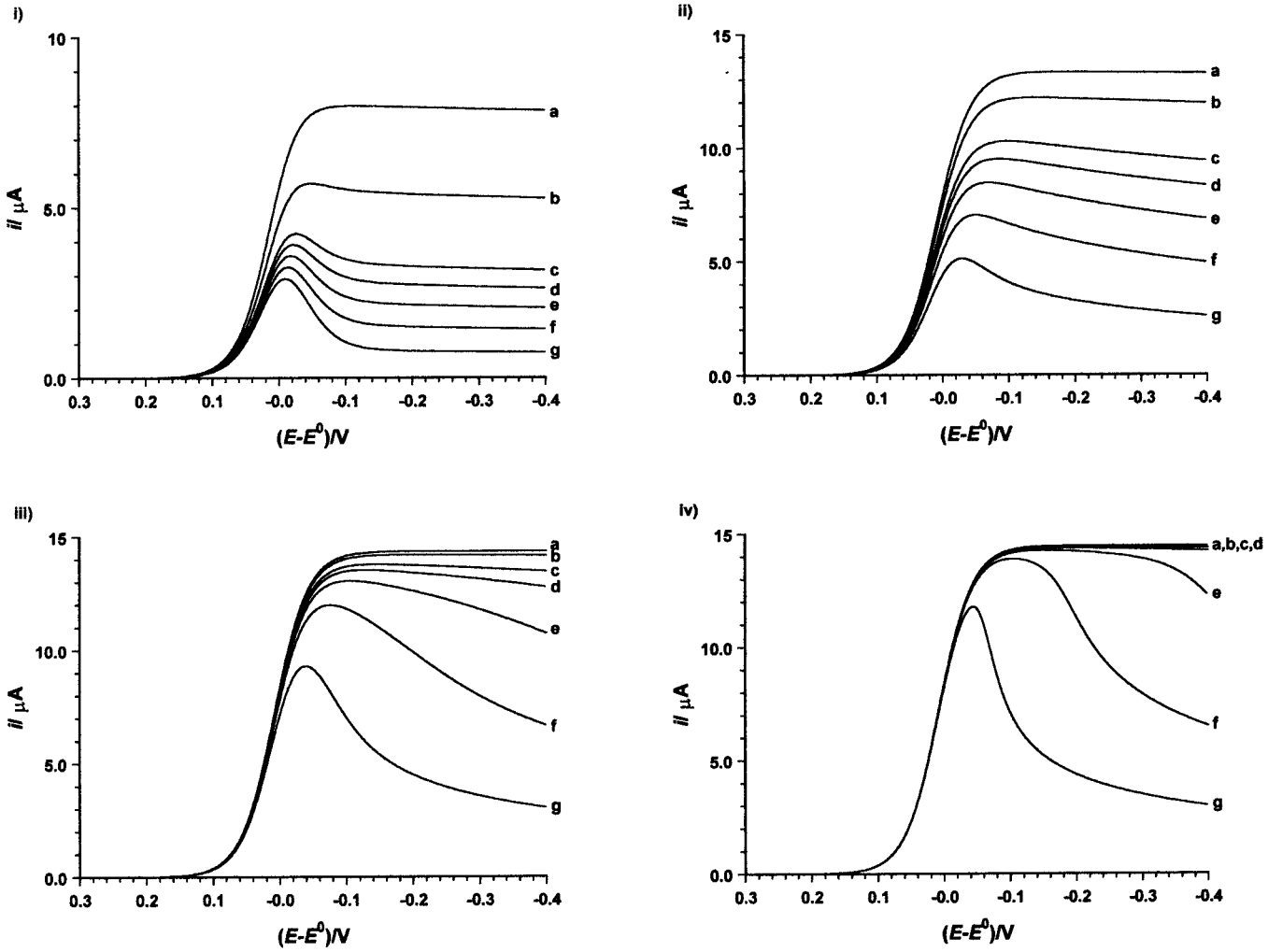


**Figure 4.** Simulated voltammograms for $k_{12}$ = (i) 0.1, (ii) 1.0, (iii) 10.0, and (iv) 100.0 cm $M^{-1}$ $s^{-1}$. In each case, $D_{Ox_1} = 2.5 \times 10^{-6}$ $cm^2$ $s^{-1}$, $D_{Red_1} = 3.0 \times 10^{-6}$ $cm^2$ $s^{-1}$, $D_{Ox_2} = 7.5 \times 10^{-6}$ $cm^2$ $s^{-1}$, $C^*_{Ox_1} = 0.55$ mM, $d = 32$ $\mu$m, $A = 0.32$ $cm^2$, $\upsilon_s = 5$ mV $s^{-1}$, and $K_r$ takes the values (a) 20.0, (b) 10.0, (c) 5.0, (d) 4.0, (e) 3.0, (f) 2.0, and (g) 1.0.

$$\gamma_j = D_j/D_{Ox_1} \qquad \text{where } j \text{ denotes } Ox_1, Red_1 \text{ or } Ox_2 \tag{19}$$

$$\tau = (tD_{Ox_1})/d^2 \tag{20}$$

$$Z = z/d \tag{21}$$

$$K_r = c^*_{Ox_2}/c^*_{Ox_1} \tag{22}$$

$$K = (k_{12}dc^*_{Ox_2})/D_{Ox_1} \tag{23}$$

$$\sigma = \left(\frac{nF}{RT}\right)\left(\frac{\upsilon_s d^2}{D_{Ox_1}}\right) \tag{24}$$

The last of these terms, $\sigma$, is a normalized scan rate, while $K$ is the normalized rate constant for the ET process at the ITIES. It should be apparent how these terms affect the diffusion equations (eqs 6−8) and the related boundary and initial conditions outlined above.

The time-dependent current is related to the flux of $Ox_1$ normal to the electrode surface at time $t$.

$$i(t) = \frac{nFAD_{Ox_1}c^*_{Ox_1}}{d}\left(\frac{\partial C_{Ox_1}}{\partial Z}\right)_{Z=0} \tag{25}$$

**Method of Solution**

Numerical solutions were achieved using the explicit finite-difference method to calculate the current−potential behavior and the concentration profiles of the species in the two phases. A detailed account of the application of this method for semiinfinite linear diffusion problems has been given elsewhere.[17] For the present model, the one-dimensional finite-difference grid adopted was similar to that used previously by us for the $z$-coordinate for two-dimensional two-phase problems.[12,19] A linear grid was constructed for the electrode/ITIES domain over the thin layer (phase 1), whereas for the bulk solution (phase 2) the $z$-coordinate was transformed with an exponential-expanding function of the form[20]

$$\xi = \ln[1 + B(Z - 1)] \tag{26}$$

The value of the grid expansion coefficient $B$ was chosen so that the grid spacings of the uniform and expanding grids were matched at the interface. The grid spacing in phase 2 was therefore wider with increasing distance from the liquid/liquid interface, improving the efficiency of the simulation by increasing the proportion of grid points in regions where the concentration gradient was steepest. To ensure a stable simulation, a fixed time step was employed, $\Delta\tau$, which was calculated according to the criteria that the coefficient $\lambda_1$ for each phase had a value $\leq 0.45$,[17] where $\lambda_i$ for phase $i$ ($i = 1$ or 2) is dependent on the

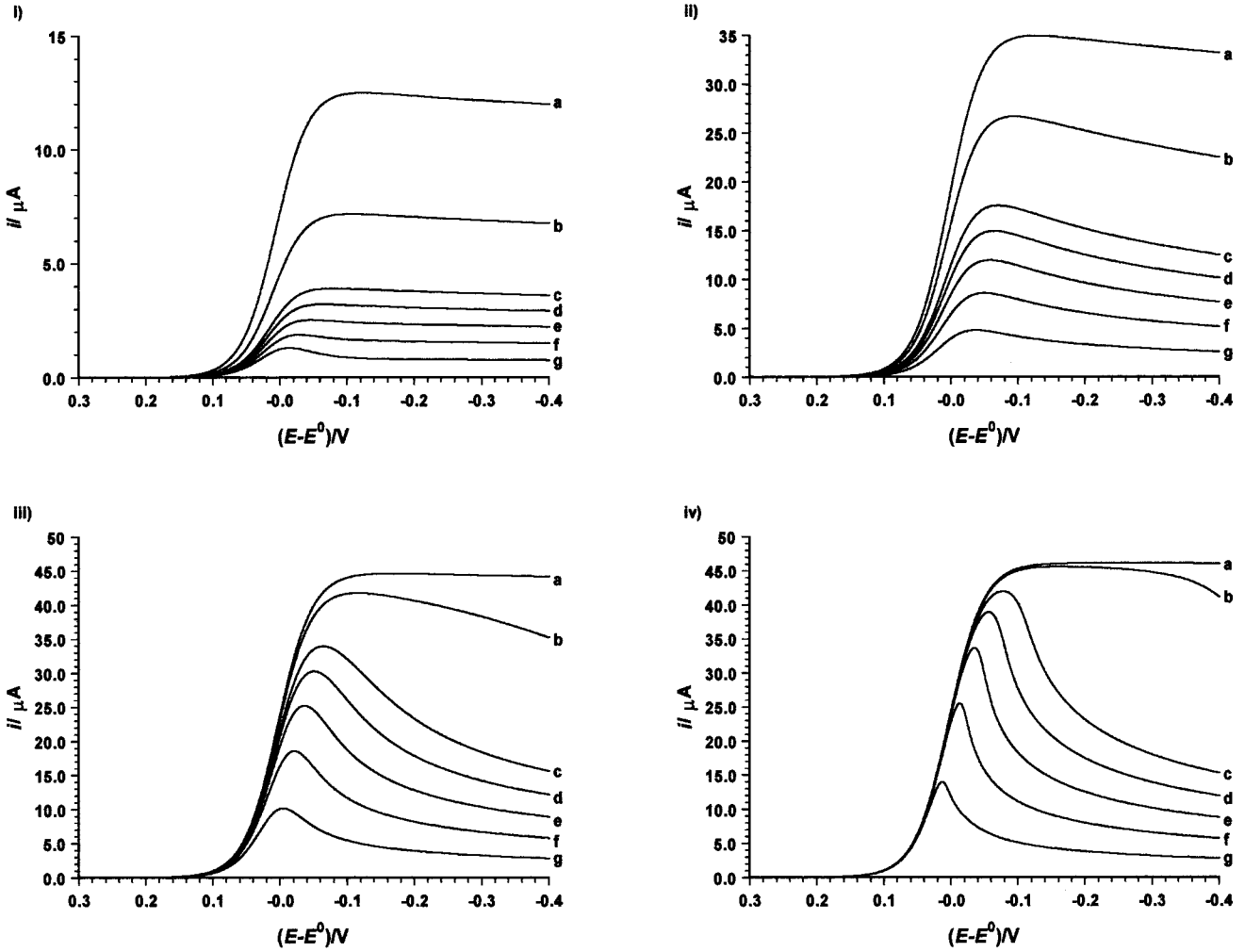


**Figure 5.** Simulated voltammograms for $k_{12}$ = (i) 0.1, (ii) 1.0, (iii) 10.0, and (iv) 100.0 cm $M^{-1}$ $s^{-1}$. In each case, $D_{Ox_1} = 2.5 \times 10^{-6}$ $cm^2$ $s^{-1}$, $D_{Red_1} = 3.0 \times 10^{-6}$ $cm^2$ $s^{-1}$, $D_{Ox_2} = 7.5 \times 10^{-6}$ $cm^2$ $s^{-1}$, $C^*_{Ox_1} = 0.55$ mM, $d = 10$ $\mu$m, $A = 0.32$ $cm^2$, $\upsilon_s = 5$ mV $s^{-1}$, and $K_r$ takes the values (a) 20.0, (b) 10.0, (c) 5.0, (d) 4.0, (e) 3.0, (f) 2.0, and (g) 1.0.

diffusion coefficient of the species and the grid spacing $\Delta Z_i$:

$$\lambda_1 = \gamma_{Ox_1} \frac{\Delta\tau}{(\Delta Z_1)^2} \tag{27}$$

$$\lambda_2 = \gamma_{Ox_2} \frac{\Delta\tau}{(\Delta Z_2)^2} \tag{28}$$

In dimensionless finite-difference form, the boundary condition (eq 15) at the ITIES becomes

$$C_{Ox_1,NZ1} = C_{Ox_1,NZ1-1} + K\Delta Z_1 C_{Red_1,NZ1} C_{Ox_2,NZ1} \tag{29}$$

$$C_{Red_1,NZ1} = \frac{C_{Red_1,NZ1-1}}{\left(1 + \frac{K\Delta Z_1}{\gamma_{Red_1}} C_{Ox_2,NZ1}\right)} \tag{30}$$

$$C_{Ox_2,NZ1} = \frac{C_{Ox_2,NZ1+1}}{\left(1 + \frac{K\Delta Z_2}{K_r \gamma_{Ox_2}} C_{Red_1,NZ1}\right)} \tag{31}$$

where NZ1 is the number of grid points over phase 1. It is clear that the calculation of new concentrations of the species of interest involves equations that are interdependent. For each new time step, this problem was circumvented by implementing an iterative procedure in which $C_{Ox_2,NZ1}$ in eq 30 and $C_{Red_1,NZ1}$ in eq 31 were initially approximated by the corresponding values calculated for the previous time step. After evaluating $C_{Red_1,NZ1}$ from eq 30 and $C_{Ox_2,NZ1}$ from eq 31, the procedure was repeated using the newly determined concentrations until the concentrations of $Red_1$ and $Ox_2$ at the ITIES were unchanged (within a precision of $10^{-16}$) on further iteration. The concentration of $Ox_1$ at the interface could then be calculated from eq 29.

The program for the simulation was written in FORTRAN and run on the University of Warwick central UNIX system.

## Theoretical Results and Discussion

The theoretical treatment presented above involves a number of parameters, including the concentration and diffusion coefficients of the species in the two phases, the rate constant for electron transfer at the liquid/liquid interface, the thickness of the thin layer, and the scan rate. The aim of this section is to assess the conditions under which diffusion in phase 2 has an effect on the voltammetric behavior and the applicability of eq 2 in analyzing experimental data.

Owing to the large number of variables, parameter values were examined that were relevant to the experimental

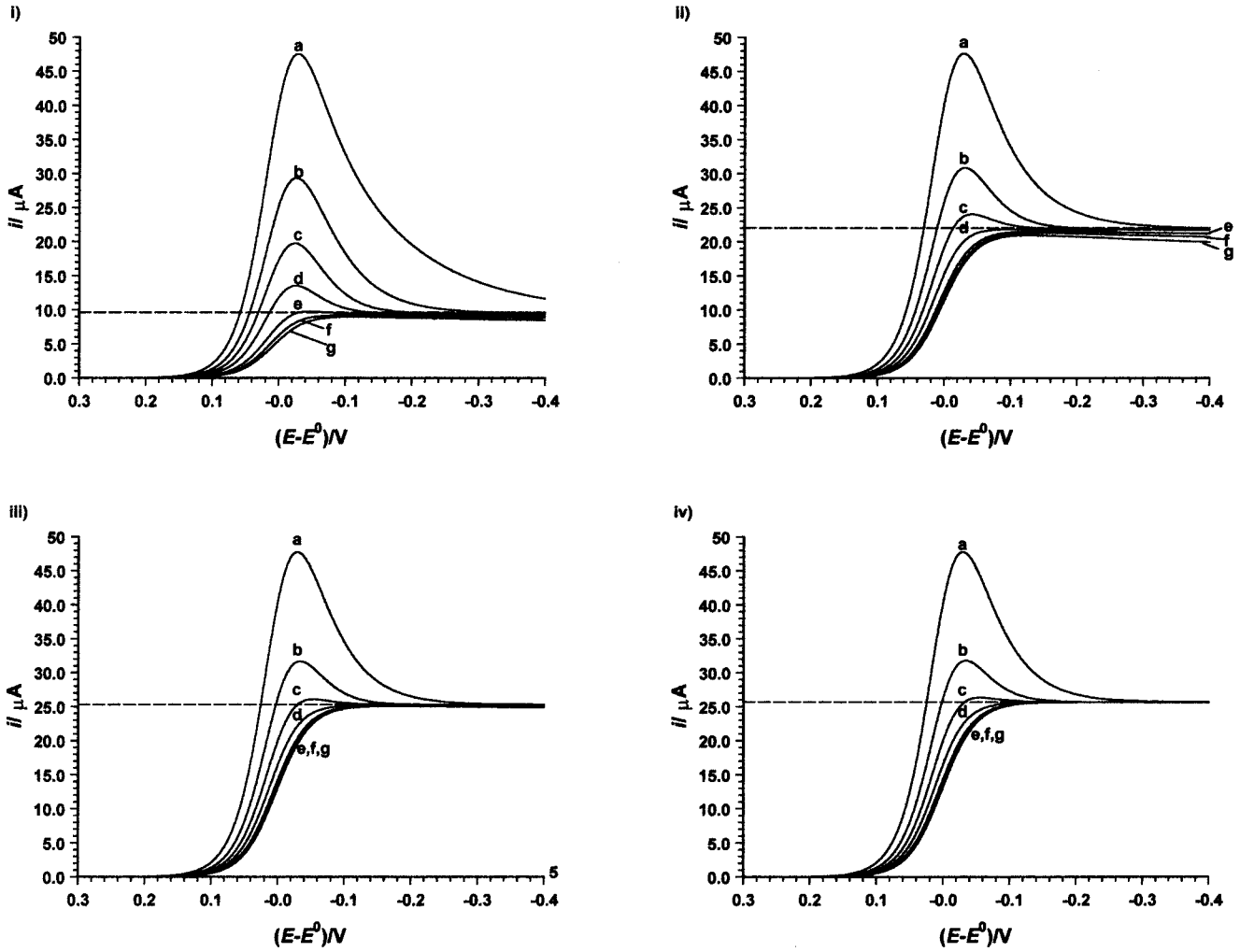


**Figure 6.** Simulated voltammograms for $k_{12}$ = (i) 0.1, (ii) 1.0, (iii) 10.0, and (iv) 100.0 cm $M^{-1}$ $s^{-1}$. In each case, $D_{Ox_1} = D_{Red_1} = D_{Ox_2} = 2.5 \times 10^{-6}$ $cm^2$ $s^{-1}$, $C^*_{Ox_1} = 0.5$ mM, $d = 15$ $\mu$m, $A = 0.32$ $cm^2$, $K_r = 20.0$, and $\upsilon_s$ takes the values (a) 500, (b) 200, (c) 100, (d) 50, (e) 20, (f) 10, and (g) 5 mV $s^{-1}$. The predicted steady-state limiting currents from the constant-composition model (eq 2) are shown as the dashed lines for comparison.

investigation of the ET process between decamethyferrocene (DCMFc) and ferricyanide across the nitrobenzene/aqueous interface, reported in ref 9b. The reaction at the interface is

$$DCMFc_{(NB)} + Fe(CN)_6^{3-}{}_{(aq)} \rightarrow DCMFc^+{}_{(NB)} + Fe(CN)_6^{4-}{}_{(aq)} \quad (32)$$

In this study, the thin film of nitrobenzene adhered to the graphite electrode was determined to have a thickness of 32 $\mu$m and contained 0.55 mM $DCMFc^+$, electrogenerated prior to the voltammetric scan from the oxidation of DCMFc at the initial potential. The graphite working electrode had an area of 0.32 $cm^2$, and the diffusion coefficient of DCMFc was measured by cyclic voltammetry to be $6 \times 10^{-6}$ $cm^2$ $s^{-1}$.[9b] For concentrations of ferricyanide, equivalent to $K_r \sim 1-20$, the voltammetric response of the electrode, at a scan rate of 5 mV $s^{-1}$, was considered to attain a steady-state plateau current, which was fitted to eq 2 to yield a value for the ET rate constant at the ITIES of 0.9 cm $M^{-1}$ $s^{-1}$. This value was found to be virtually independent of the potential drop across the interface.

Simulations were performed using the full model presented above, for comparison to this experimental investigation, assuming $D_{Ox_1} = D_{Red_1} = 6.0 \times 10^{-6}$ $cm^2$ $s^{-1}$ and $D_{Red_2} = 7.5 \times 10^{-6}$ $cm^2$ $s^{-1}$, the previously measured value for the diffusion coefficient of ferricyanide.[21]

The effect on the voltammetric response of varying $K_r$, for four rate constants, is shown in Figure 2i−iv. The values of $k_{12}$ were chosen to represent the range of values typically encountered in experimental studies of ET rates across an ITIES. The predicted plateau currents, calculated from eq 2, assuming a constant composition in phase 2 are also plotted in each case for comparison.

A key feature of the simulated voltammograms in Figure 2 is that as the potential is scanned past $E°$, the current generally rises to a maximum value, which is dependent on the values of $k_{12}$ and $K_r$. Under the defined conditions, a steady-state current is hardly ever attained, except for the highest values of $K_r$, i.e., $K_r \geq 20$. Even for the lowest rate constant, $k_{12} = 0.1$ cm $M^{-1}$ $s^{-1}$ in Figure 2i, broad peaks are evident in the voltammograms, close to $E°$, for $K_r \leq 5$.

For all kinetic cases, the deviation of the voltammetric response from that predicted by the constant-composition model increases as $K_r$ is reduced, indicating that diffusional limitations of $Ox_2$ in phase 2 become more important. For a fixed value of $K_r$ this deviation is more pronounced as $k_{12}$ is increased, reflected by both the enhanced peak heights and narrower peaks widths of the simulated voltammograms in Figure 2iv for $K_r \leq 5$. The sensitivity of the peak height and shape to the value of the rate constant suggests that the use of low concentrations in phase 2 may be advantageous for the measurement of faster kinetics

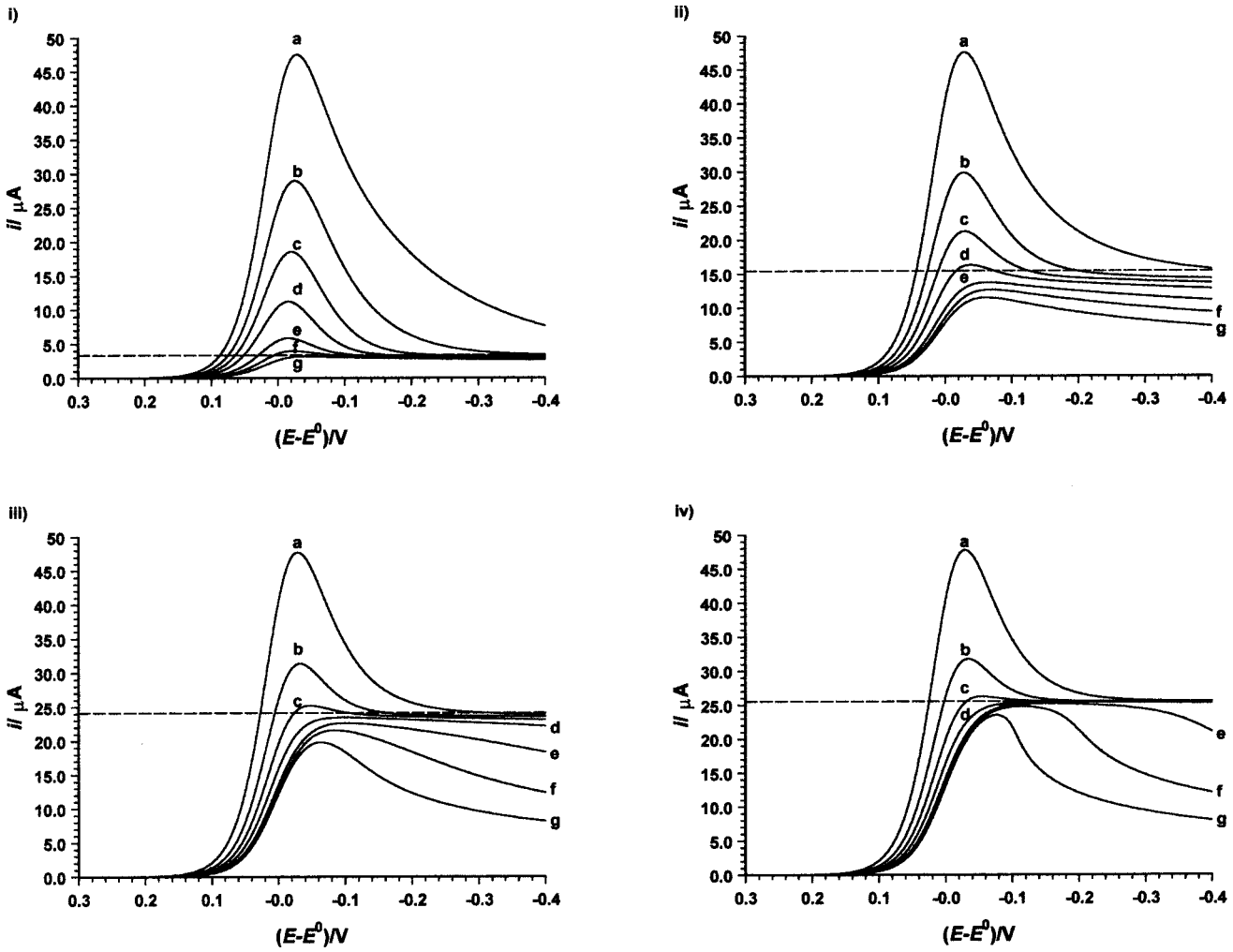


**Figure 7.** Simulated voltammograms for $k_{12}$ = (i) 0.1, (ii) 1.0, (iii) 10.0, and (iv) 100.0 cm $M^{-1}$ $s^{-1}$. In each case, $D_{Ox_1} = D_{Red_1} = D_{Ox_2} = 2.5 \times 10^{-6}$ $cm^2$ $s^{-1}$, $C^*_{Ox_1} = 0.5$ mM, $d = 15$ $\mu$m, $A = 0.32$ $cm^2$, $K_r = 5.0$, and $\upsilon_s$ takes the values (a) 500, (b) 200, (c) 100, (d) 50, (e) 20, (f) 10, and (g) 5 mV $s^{-1}$. The predicted steady-state limiting currents from the constant-composition model (eq 2) are shown as the dashed lines for comparison.

using this approach, a point that is discussed later. For high values of $K_r$ and fast kinetics, the current rises to a limiting value of 31.8 $\mu$A (Figure 2iv), which is consistent with the value calculated from eq 3, under conditions where there is no kinetic barrier to ET at the ITIES and the observed current is limited only by the rate of diffusion of the species in the thin layer.

The reason for the breakdown of eq 2 is revealed when the simulated concentration profiles of the redox species in the two phases are examined at various points along a voltammogram. Figures 3i−iii shows the concentration distribution of $Ox_1$, $Red_1$, and $Ox_2$ at potentials corresponding to the peak current and at −0.1 V and −0.3 V vs $E°$ for three rate constants, with $K_r = 2$ fixed. In all three plots, the peak current corresponds to the steepest concentration gradient of $Ox_1$ and therefore the greatest rate of mass transfer at the electrode surface.

In the slow kinetic regime with $k_{12} = 0.1$ cm $M^{-1}$ $s^{-1}$, Figure 3i, the rate of regeneration of $Ox_1$ at the ITIES is low. The initial rise in the current as the potential is scanned passed $E°$ is followed by a sharp decrease as $Ox_1$ in the thin layer is rapidly consumed by electrolysis. As the potential is scanned beyond −0.1 V vs $E°$, the depletion of $Ox_2$ in phase 2 at the ITIES becomes more apparent and the current continues to decrease gradually (although experimentally this could be misinterpreted as a steady-state current). By −0.4 V vs $E°$, the concentration of $Ox_2$ at the interface has fallen to ∼83% of its initial value. Although the depletion of $Ox_2$ at the interface seems slight, the deviation of the current from that predicted by the constant-composition model indicates that diffusional limitations in phase 2 have an effect, even for low rate constants. As $k_{12}$ is increased, the rate of turnover of $Ox_1$ at the interface becomes progressively more rapid ($k_{12} = 1$ cm $M^{-1}$ $s^{-1}$ in Figure 3ii and $k_{12} = 100$ cm $M^{-1}$ $s^{-1}$ in Figure 3iii). Consequently, in the region near to the ITIES, the concentration of $Ox_1$ in the thin layer is initially high and the concentration of $Ox_2$ is depleted, as illustrated by the concentration profile in Figure 3iii at the peak current. As the potential is swept further, the depletion of $Ox_2$ close to the liquid/liquid interface becomes more severe, decreasing the rate of regeneration of $Ox_1$ at the ITIES and diminishing the concentration of $Ox_1$ in the thin layer at the electrode surface. A steady-state concentration profile within the thin layer is not achieved.

The kinetic case shown in Figure 3ii is close to the suggested value for the ET rate constant between decamethylferrocene and ferricyanide in ref 9b. It should be noted that for this system the assumption that phase 2 is maintained at a constant composition has been applied to analyze data characterized by $K_r$ values lower than 2. The plot in Figure 3ii shows that, for these conditions, significant depletion is expected to occur adjacent to the liquid/liquid interface and that it is not valid to

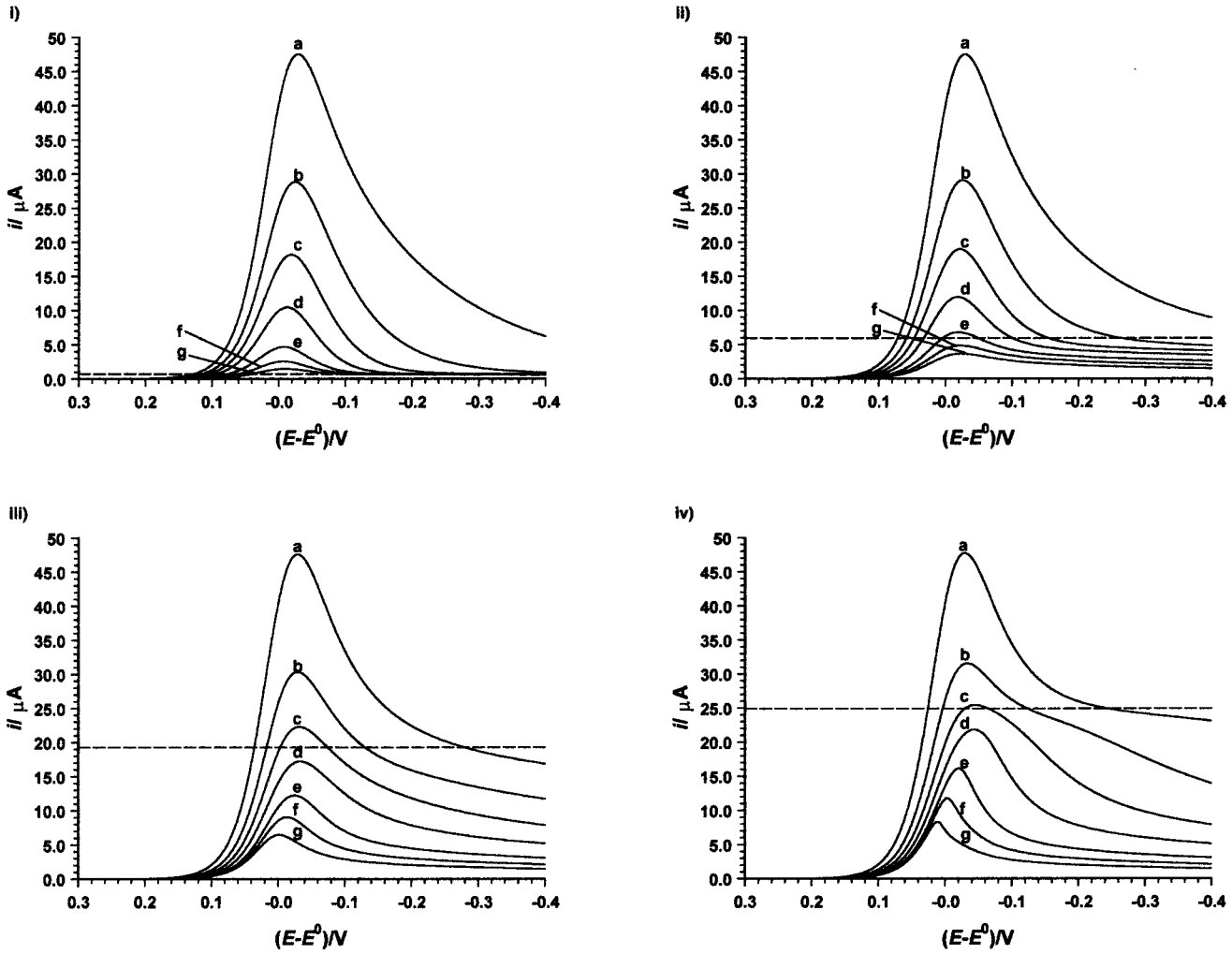


**Figure 8.** Simulated voltammograms for $k_{12}$ = (i) 0.1, (ii) 1.0, (iii) 10.0, and (iv) 100.0 cm $M^{-1}$ $s^{-1}$. In each case, $D_{Ox_1} = D_{Red_1} = D_{Ox_2} = 2.5 \times 10^{-6}$ $cm^2$ $s^{-1}$, $C^*_{Ox_1} = 0.5$ mM, $d = 15$ $\mu$m, $A = 0.32$ $cm^2$, $K_r = 1.0$, and $\upsilon_s$ takes the values (a) 500, (b) 200, (c) 100, (d) 50, (e) 20, (f) 10, and (g) 5 mV $s^{-1}$. The predicted steady-state limiting currents from the constant-composition model (eq 2) are shown as the dashed lines for comparison.

assume that the thin layer has a steady-state concentration profile.

Recent work has shown that for a number of electrochemical techniques the assumption of equal diffusion coefficients for the oxidized and reduced form of a redox couple is not always appropriate.[22−24] Since the model above predicts the voltammetric response to be highly dependent on the rate of diffusion of the species in the thin layer, we determined the ratio of the diffusion coefficients for the $DCMFc^+$/DCMFc redox couple by ultramicroelectrode single and double potential step chronoamperometry.[23] Under similar conditions to those used in the studies of ref 9b, we found quite different diffusion coefficients than assumed:[9b] $D_{DCMFc} = 3.0\ (\pm 0.05) \times 10^{-6}$ $cm^2$ $s^{-1}$, $D_{DCMFc^+} = 2.5\ (\pm 0.1) \times 10^{-6}$ $cm^2$ $s^{-1}$, and thus $\gamma_{Red_1} = 0.8$ (as defined in eq 19).[25]

Figure 4 shows simulated voltammograms using these values for the diffusion coefficients of the species in the thin layer: the other parameters are assigned values as detailed in the above. From these plots it can be seen that for the four kinetic cases considered previously in Figure 2, the general features are similar. It is apparent in Figure 4 that the lower rate of diffusion in the thin layer results in decreased current and a decrease in the value of $K_r$ required for the attainment of a steady state. In the limit of high $K_r$ and moderate-to-fast kinetics, the current approaches a plateau value of 14.46 $\mu$A. This is in agreement with the value of 14.47 $\mu$A, calculated from eq 33, for the steady-state diffusion-limited current of a twin-electrode thin-layer cell, under the defined conditions.[26]

$$i_D = nFAc^*_{Ox_1}\frac{2D_{Ox_1}D_{Red_1}}{(D_{Ox_1} + D_{Red_1})d} \qquad (33)$$

Extraction of kinetic parameters for the ET process at the ITIES from experimental data, using either the full model described here or the approximation of eq 2, requires a precise knowledge of the thickness of the thin layer adhered to the electrode. This was determined in ref 9a via the concentration, by determining the ratio of the peak current of the voltammetric response under thin-layer and semiinfinite diffusion-limited conditions by employing, respectively, either a slow scan rate so that the reactant in the thin layer was completely consumed or a fast scan rate so that the diffusion layer was smaller than the thickness of the film. The latter method, of course, requires an accurate knowledge of the diffusion coefficient. This approach produced results consistent with the value of the thickness of the thin layer calculated from the volume of the organic solvent used to prepare the film. To examine the effect of varying the thin-layer thickness in the full model, voltammograms were simulated for the same conditions as for Figure 4, except the thickness of the thin layer was reduced to 10 $\mu$m. The more rapid mass transfer across a thinner film results in a

higher rate of regeneration of $DCMFc^+$ at the ITIES via the ET process and an increased depletion of the redox species in the aqueous phase at the interface. Hence, the voltammetric responses in Figure 5 are characterized by higher currents and greater sensitivity to the value of $K_r$ compared to the corresponding cases in Figure 4. For the moderate-to-fast kinetic cases in Figure 5, the steady-state approximation represented by eq 2 is seen to only be valid for $K_r \geq 20$.

As a final application of the full model, the effect of changing the scan rate on the voltammetric response was investigated. It is beyond the scope of this paper to provide a complete set of working curves, given the large number of possible parameters, and therefore the following discussion aims to give a general guide of the effects of scan speed and the implications for the measurement of fast ET kinetics. Simulated voltammograms were obtained for an example case for which $D_{Ox_1} = D_{Red_2} = D_{Ox_2} = 2.5 \times 10^{-6}$ cm$^2$ s$^{-1}$, $C^*_{Ox_1} = 0.5$ mM, $d = 15$ $\mu$m, and $A = 0.32$ cm$^2$.

Figure 6 shows the effect of scan speed on the voltammetric response for four rate constants, with $K_r = 20$ (large excess of $Ox_2$ in the second phase to $Ox_1$ in the thin layer). It can be seen that for fast kinetics (Figure 6iv) and slow scan speeds the current rises to a plateau value that agrees with that predicted by eq 2. For faster scan rates ($\upsilon_s > 100$ mV s$^{-1}$) the voltammograms are peaked, but the current then rapidly approaches the steady-state approximation. As $k_{12}$ is reduced, depletion effects become more apparent for the slowest scan speed but for fast scan speeds the current again approaches the steady-state value. It should be noticed that although there are slight differences between the curves for $k_{12} = 10$ cm M$^{-1}$ s$^{-1}$ and $k_{12} = 100$ cm M$^{-1}$ s$^{-1}$ (Figure 6iii,iv), these would be difficult to determine practically. Even a small rate constant $k_{12} = 1$ cm M$^{-1}$ s$^{-1}$ (Figure 6ii) gives a plateau current of 22.05 $\mu$A that is only slightly smaller than the value of 25.31 $\mu$A in Figure 6iii for $k_{12} = 10$ cm M$^{-1}$ s$^{-1}$. This has obvious experimental implications: if a large excess of the redox species is employed in the second phase, then under these conditions it would only be possible to determine a rate constant of the order of 1 cm M$^{-1}$ s$^{-1}$ or less, with the other parameters as defined. For thicker layers, this problem is exacerbated.

The simulated voltammograms for $K_r = 5$, in Figure 7, show similar trends. The constant-composition assumption is only valid for the slowest kinetic case (Figure 7i) and is found to break down as $k_{12}$ is increased, except for the fastest scan rates, where the voltammetric response rises to a peak before declining to a limiting value that is close to the approximation. These effects become more pronounced as $K_r$ is reduced further to $K_r = 1$, in Figure 8. These data illustrate that the constant-composition approximation of eq 2 does not hold for low values of $K_r$ for the defined conditions and for scan rates typically employed in experiments. Nevertheless, there are measurable differences in the peak heights and shapes of the voltammetric responses corresponding to the four kinetic cases in Figure 8. In particular, there are discernible differences in the voltammetric responses for $k_{12} = 10$ cm M$^{-1}$ s$^{-1}$ and $k_{12} = 100$ cm M$^{-1}$ s$^{-1}$ for all scan rates. This suggests that by dropping the concentration of the redox species in the second phase and using a range of potential scan rates, the measurement of faster kinetics becomes more accessible.

## Conclusions

A full model for the thin-layer method used to study ET rates at ITIES has been developed, showing that an earlier approximate treatment[9b,c] (eq 2) is invalid under the experimental conditions used thus far, unless a high excess of the redox-active species is employed in phase 2. The significant depletion effects observed at low $K_r$ mean that the full analysis developed in this paper is needed if the thin-layer method is to provide accurate information. A copy of the Fortran program used for these simulations is available from the authors on request. It is clear that under the experimental conditions, reported in ref 9b, where eq 2 is valid, a rate constant of 1 cm M$^{-1}$ s$^{-1}$ is close to the diffusional limit, and it would be difficult to measure faster kinetics. It may be that the previously reported $k_{12}$ values simply represent this limit, rather than a potential independence of $k_{12}$.

The results in this paper show that there are possible advantages to employing low $K_r$ to measure faster kinetics, because distinctive voltammograms are obtained with different peak heights and widths that appear to be kinetically diagnostic. The thin-layer method could thus be further optimized by employing a range of values of $K_r$ and scan speeds. It should be emphasized generally, however, that the experimental method does require an accurate knowledge of the layer thickness and the diffusion coefficients of the reactants. Careful consideration needs to be given to determining these parameters in practice.

Our results show that for most practical conditions diffusion in phase 2 is important, with the implication that problems from natural convection may result under slow scan speed conditions used hitherto. This type of problem has been excluded from the discussion in this paper, but clearly it maybe advantageous to employ shorter time scales when depletion effects become significant. Additionally, it is worth emphasizing that general consideration needs to be given to the distribution potential in small systems, such as this thin-layer method, as outlined elsewhere.[27]

**Acknowledgment.** We are grateful to the EPSRC (GR/L15074) for support of this work.

## References and Notes

(1) For reviews, see: (a) Girault, H. H.; Schiffrin, D. J. In *Electroanalytical Chemistry*; Bard, A. J., Ed.; Marcel Dekker: New York, 1989; Vol. 15. (b) Girault, H. H. In *Modern Aspects of Electrochemistry*; Bockris, J. O'M., Conway, B. E., White, R. E., Eds.; Plenum Press: New York, 1993; Vol. 25.

(2) (a) Koryta, J. *Electrochim. Acta* **1984**, *29*, 445. (b) Koryta, J. *Electrochim. Acta* **1988**, *33*, 189.

(3) Samec, Z.; Marecek, V.; Weber, J.; Homolka, D. *J. Electroanal. Chem.* **1981**, *126*, 105.

(4) Girault, H. H.; Schiffrin, D. J. In *Charge and Field Effects in Biosystems*; Allen, M. J., Usherwood, P. N. R., Eds.; Abacus Press: Tunbridge Wells, U.K., 1984.

(5) (a) Marcus, R. A. *J. Phys. Chem.* **1990**, *90*, 1050. (b) Marcus, R. A. *J. Phys. Chem.* **1990**, *94*, 4152; *J. Phys. Chem.* **1990**, *94*, 7742 (addendum). (c) Marcus, R. A. *J. Phys. Chem.* **1991**, *95*, 2010; *J. Phys. Chem.* **1995**, *99*, 5742 (addendum).

(6) Kharkats, Yu. I.; Volkov, A. G. *J. Electroanal. Chem.* **1985**, *184*, 435.

(7) Girault, H. H.; Schiffrin, D. J. *J. Electroanal. Chem.* **1988**, *244*, 15.

(8) Samec, Z. *J. Electroanal. Chem.* **1979**, *99*, 197.

(9) (a) Shi, C.; Anson, F. C. *Anal. Chem.* **1998**, *70*, 3114. (b) Shi, C.; Anson, F. C. *J. Phys. Chem. B* **1998**, *102*, 9850. (c) Shi, C.; Anson, F. C. *J. Phys. Chem. B* **1999**, *103*, 6283.

(10) Liu, B.; Mirkin, M. V. *J. Am. Chem. Soc.* **1999**, *121*, 8352.

(11) (a) Wei, C.; Bard, A. J.; Mirkin, M. V. *J. Phys. Chem.* **1995**, *99*, 16033. (b) Tsionsky, M.; Bard, A. J.; Mirkin, M. V. *J. Phys. Chem.* **1996**, *100*, 17881. (c) Tsionsky, M.; Bard, A. J.; Mirkin, M. V. *J. Am. Chem. Soc.* **1997**, *119*, 10785. (d) Delville, M.-H.; Tsionsky, M.; Bard, A. J. *Langmuir* **1998**, *14*, 2774.

(12) Barker, A. L.; Unwin, P. R.; Zhou, J.; Amemiya, S.; Bard, A. J. *J. Phys. Chem. B* **1999**, *103*, 7260.

(13) (a) Dryfe, R. A. W.; Webster, R. D.; Coles, B. A.; Compton, R. G. *J. Chem. Soc., Chem. Commun.* **1997**, 779. (b) Webster, R. D.; Dryfe, R. A. W.; Coles, B. A.; Compton, R. G. *Anal. Chem.* **1998**, *70*, 792.

(14) (a) Ding, Z.; Fermin, D. J.; Brevet, P.-F.; Girault, H. H. *J. Electroanal. Chem.* **1998**, *458*, 139. (b) Fermin, D. J.; Ding, Z.; Duong, H. D.; Brevet, P.-F.; Girault, H. H. *J. Chem Soc., Chem. Commun.* **1998**, 1125. (c) Fermin, D. J.; Ding, Z.; Duong, H. D.; Brevet, P.-F.; Girault, H. H. *J. Phys. Chem. B* **1998**, *102*, 10334.

(15) (a) Slevin, C. J.; Unwin, P. R. *Langmuir* **1999**, *15*, 7361. (b) Zhang, J.; Slevin, C. J.; Unwin, P. R. *J. Chem. Soc., Chem. Commun.* **1999**, 1501.

(16) Andrieux, C. P.; Savéant, J.-M. In *Molecular Design of Surfaces*; Murray, R. W., Ed.; John Wiley & Sons: New York, 1992.

(17) Britz, D. *Digital Simulation in Electrochemistry*, 2nd, revised, and extended ed.; Springer-Verlag: Berlin, 1988.

(18) Bard, A. J.; Faulkner, L. R. *Electrochemical Methods*; John Wiley & Sons: New York, 1980.

(19) Barker, A. L.; Macpherson, J. V.; Slevin, C. J.; Unwin, P. R. *J. Phys. Chem. B* **1998**, *102*, 1586.

(20) Joslin, T.; Pletcher, D. J. *J. Electroanal. Chem.* **1974**, *49*, 172.

(21) Adams, R. N. *Electrochemistry of Solid Electrodes*, 1st ed.; Marcel Dekker: New York, 1969.

(22) (a) Martin, R. D.; Unwin, P. R. *J. Electroanal. Chem.* **1997**, *439*, 123. (b) Martin, R. D.; Unwin, P. R. *Anal. Chem.* **1998**, *70*, 276.

(23) (a) Macpherson, J. V.; Unwin, P. R. *Anal. Chem.* **1997**, *69*, 2063. (b) Slevin, C. J.; Macpherson, J. V.; Unwin, P. R. *J. Phys. Chem. B* **1997**, *101*, 10851.

(24) (a) Compton, R. G.; Coles, B. A.; Spackman, R. A. *J. Phys. Chem.* **1991**, *95*, 4741. (b) Compton, R. G.; Coles, B. A.; Fisher, A. C. *J. Phys. Chem.* **1994**, *98*, 2441. (c) Compton, R. G.; Coles, B. A.; Gooding, J. J.; Fisher, A. C.; Cox, T. I. *J. Phys. Chem.* **1994**, *98*, 2446.

(25) Barker, A. L.; Unwin, P. R. Manuscript in preparation.

(26) (a) Anderson, L. B.; Reilley, C. N. *J. Electroanal. Chem.* **1965**, *10*, 295. (b) Hubbard, A. T.; Anson, F. C. *Electroanalytical Chemistry*; Bard, A. J., Ed.; Marcel Dekker: New York, 1970; Vol. 4.

(27) Kakiuchi, T. In *Liquid/Liquid Interfaces: Theory and Methods*; Volkov, A. G., Deamer, D. W., Eds.; CRC Press: Boca Raton, FL, 1996; p 1.